JOURNAL OF CHEMICAL EDUCATION

pubs.acs.org/jchemeduc Communication

Shortcomings of the VSEPR Model for Hypercoordinate Species and Its Presentation in General Chemistry

Annika L. Medrano, Thomas M. Gilbert,* and Christine M. Morales*

Cite This: *J. Chem. Educ.* 2023, 100, 3659−3666 Read Online

ACCESS | Metrics & More | Article Recommendations | Supporting Information

ABSTRACT: Valence shell electron pair repulsion theory (VSEPR) as explained in most textbooks predicts that substituents bonded to a central atom in $AX_nE_z^c$ species (A = main-group central atom, X = substituent, E = lone pair on central atom, c = charge) will change their X−A−X angles to bend away from the lone pairs. Exceptions have appeared in the literature, commonly arising from steric repulsions between very large substituents and less commonly from electronic factors such as multiple bonding and bond polarization. We have conducted extensive computational studies of hypercoordinate main-group molecules and ions $AX_nE_z^c$ and $AO_mX_nE_z^c$, where X = halide, and found that VSEPR-based predictions of such bending for those species containing heavier halides are likely incorrect. Indeed, despite the fact that cases where X = F usually conform to the prediction, we find that $IOF_4^-/XeOF_4$ and $IO_2F_2^-/XeO_2F_2$ should not. Calculations of the electron localization function indicate that the root cause of the difference is the migration of lone pairs closer to the central atom. We recommend that presentation of VSEPR in general chemistry and inorganic chemistry textbooks be revisited and provide suggested language incorporating this phenomenon.

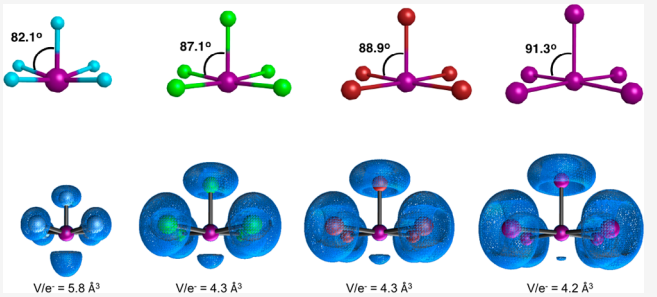

KEYWORDS: *First-Year Undergraduate/General, Second-Year Undergraduate, Upper-Division Undergraduate, Physical Chemistry, Inorganic Chemistry, Misconceptions, Computational Chemistry, Main-Group Chemistry, Molecular Properties/Structure, VSEPR Theory*

The Valence Shell Electron Pair Repulsion (VSEPR) theory developed by Gillespie has dominated chemical structure theory of main-group compounds for decades.[1,2] VSEPR concepts are taught in general chemistry courses as the primary means to predict structures of main-group compounds and ions, and VSEPR remains a "required concept" of standard training in chemistry. The model provides five basic geometries for cases where central atoms do not carry lone pairs and an additional eight derivative geometries for cases where they do. Idealized bond angles are predicted for molecules with one of the five basic geometries, and in molecules with one of the eight derivative geometries the bond angles are predicted to bend away from lone pairs. This is conceptualized in VSEPR as a "repulsion hierarchy" of lone pair−lone pair > lone pair−bonding pair ≫ bonding pair−bonding pair on central atoms.[3]

Broadly speaking, VSEPR is successful in predicting the basic structures and angle deviations. That said, anomalies/exceptions exist due to the reliance of the approach on electron−electron repulsion as dominating structural choices. VSEPR is predicated on "electron domains" portrayed as roughly equivalent in size, and commentaries on its limitations have appeared regularly.[4−7] One group of VSEPR-violating species involves substituent steric effects; $N(i\text{-}Pr)_3$ (C−N−C = 119°)[8] and $Z(t\text{-}Bu)_2$ (Z = O, S; C−O−C = 131°, C−S−C = 113°)[9,10] are examples where the substituent−central atom−substituent angles are larger than the expected 109.5°. Gillespie expanded the VSEPR approach to involve such species with his Ligand Close Packed (LCP) approach.[11] Another group arises from electronic effects like multiple bonding to peripheral atoms and bond polarization.[7] SO_2 (O−S−O = 119°)[12,13] exemplifies the effect of multiple bonding, while the NH_3/NF_3 pair, where NH_3 has a larger bond angle (106.6° vs 101.9°) despite the smaller size of the H atom,[14] exemplifies the effect of bond polarization. In such cases, steric pressure from a nonbonded "lone pair" domain is not sufficient to compress bond angles as expected. For this class, Bent's rule invokes variable hybridization of atomic orbitals to predict that bond angles increase as the electronegativity of peripheral groups decreases.[15] However, Bent's rule was formulated (and quantified by Coulson's theorem[16]) for main-group species that obey the octet rule; its application to hypercoordinate species is not established. In contrast, despite or perhaps due

Received: May 8, 2023
Revised: July 24, 2023
Published: August 17, 2023

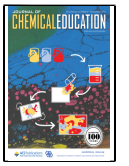

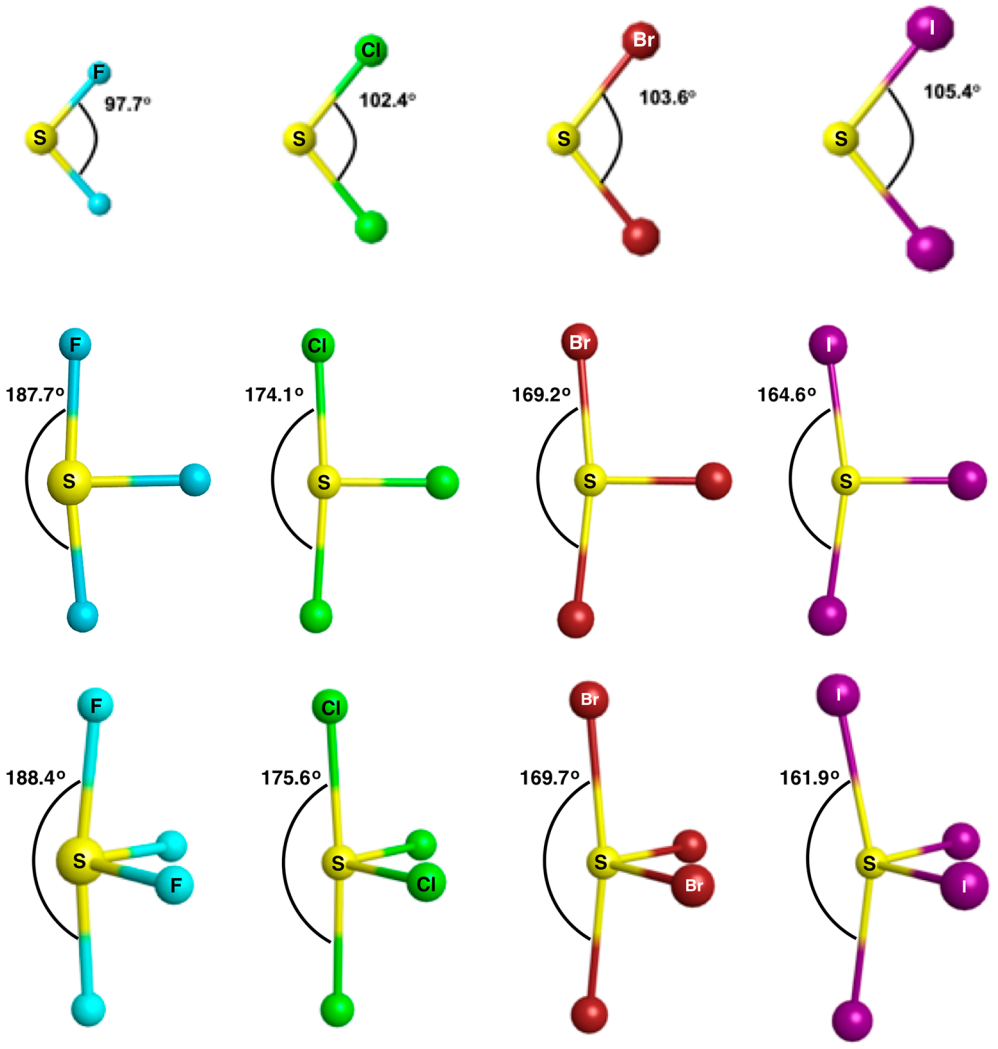

Figure 1. Optimized (M06-2X+GD3/def2-TZVP) structures of "normal coordinate" SX_2 (top) and hypercoordinate SX_3^- (middle) and SX_4 (bottom) (X = F, Cl, Br, I left to right) showing the change in the selected X−S−X angles with halide substituent size. Sulfurs are shown in yellow, fluorines in aqua, chlorines in green, bromines in red-brown, and iodines in purple. It is noteworthy that the angle change is consistent across all families yet only violates the VSEPR prediction for the hypercoordinate SX_3^- and SX_5 structures.

to its simplicity, the application of VSEPR to hypercoordinate species is seldom questioned in textbooks.

In this work, we focus on shortcomings of VSEPR predictions for hypercoordinate species containing lone pairs on the central atom ($AX_nE_z^c$/$AO_mX_nE_z^c$), specifically, those predictions associated with the repulsion hierarchy. Debates surrounding the nature of bonding in such species persist.[17−23] Possibly, standard explanations involving steric repulsion and electronegativity could be extended to explain trends in bond angles in $AX_nE_z^c$/$AO_mX_nE_z^c$ species, but unfortunately, too few experimental structural data exist to conclusively determine these trends. To our knowledge, only a handful of examples—seesaw SF_4,[24,25] SeF_4,[26] TeF_4, and $TeCl_4$;[27] $Te(CH_3)_4$;[28] and square-pyramidal $XeOF_4$[29]—have been structurally characterized in the gas phase, meaning that the structures are free of condensed-phase artifacts. Relevant to the work below, the O−Xe−F angle in $XeOF_4$ was found by microwave spectroscopy to be 91.8 ± 0.5°, meaning that the equatorial fluorine atoms bend *toward* the basal lone pair rather than away from it.[29] This violates the repulsion hierarchy prediction that the lone pair on Xe should repel the fluorines and compress the F−Xe−O angles to values below the idealized 90° angle. Solid-state structures of hypercoordinate species have appeared, mostly polyfluorides.[30−33] Usefully, the structure of PBr_4^- shows an axial Br−P−axial Br angle deviation[34,35] consistent with our quantum-chemical predictions below.

Computationally, quantum-chemical calculations from the Gilbert group and others[36] found examples of $AX_nE_z^c$/$AO_mX_nE_z^c$ species behaving like $XeOF_4$: rather than adopting bond angles that bent the substituents away from the lone pairs, the substituents bent *toward* the lone pairs. The observations raise the question of how the electronic distributions of lone and bonding pairs change with substituent size. Analysis of electron density distributions can yield meaningful insights into the usefulness of basic concepts, such as "lone pair size" and "electron pair repulsion", that often are used qualitatively to justify the extension of the simple VSEPR model to challenging chemical systems such as these. One such analysis, the electron localization function (ELF), comports well with the basic principle of repulsion.[37] The ELF is a positive quantity defined over all points in space that scales from 0 to 1, such that 0.5 corresponds to a uniform electron gas (see the Supporting Information for a mathematical treatment). Within this framework, "electron domains" can be

https://doi.org/10.1021/acs.jchemed.3c00415
J. Chem. Educ. 2023, 100, 3659−3666

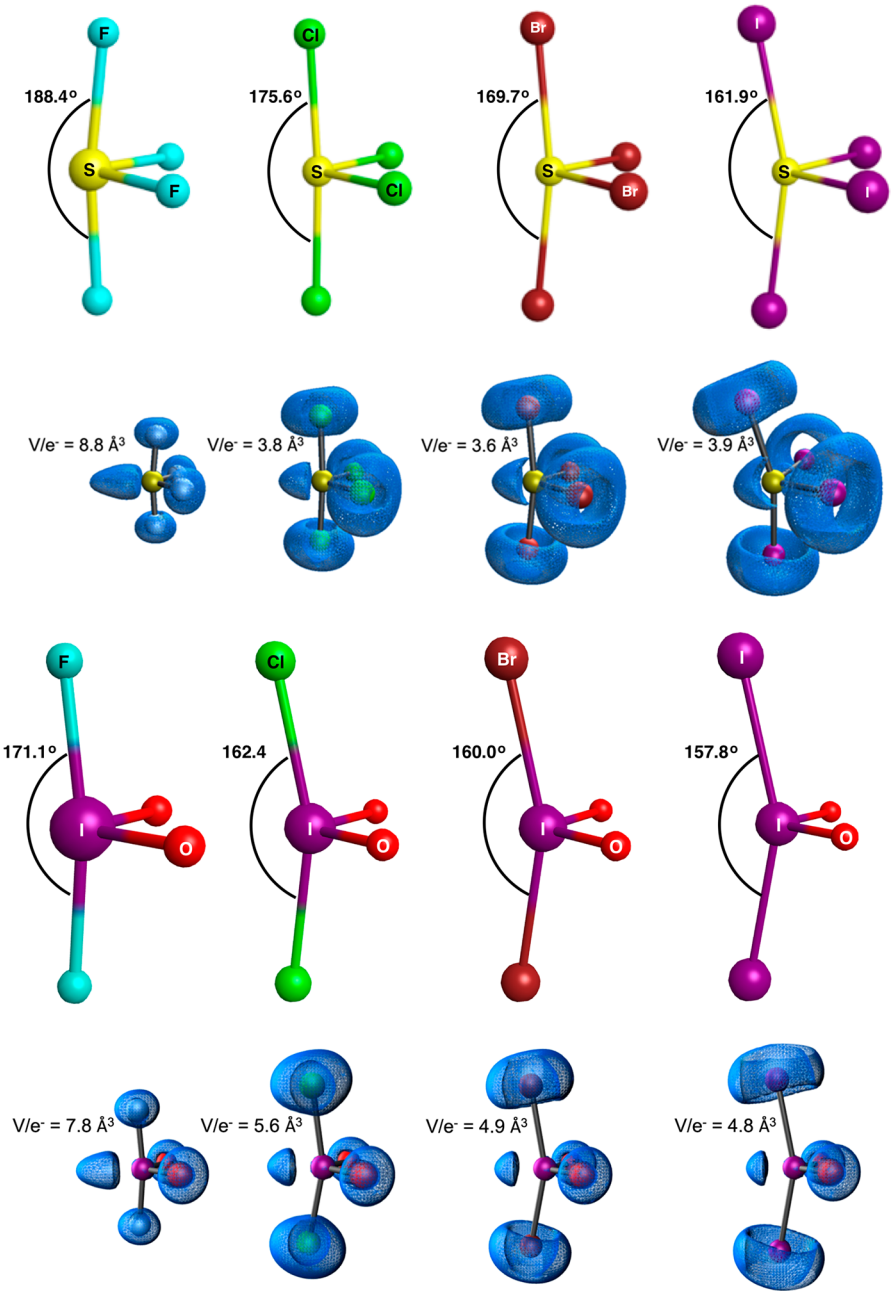

Figure 2. Optimized (M06-2X+GD3/def2-TZVP) structures and associated ELF isosurfaces (η = 0.8) of (top) SX_4 and (bottom) $IO_2X_2^-$ (X = F, Cl, Br, I) showing the change in the X_{axial}−A−X_{axial} angle with halide substituent size. Oxygens are shown in red, sulfurs in yellow, fluorines in aqua, chlorines in green, bromines in red-brown, and iodines in purple. The lone pair on A points to the left, and the corresponding nonbonded basins extend to the left of A. V/e^- is the nonbonded basin volume per electron (η = 0.02). For SI_4 and to a lesser extent SBr_4, V/e^- appears to include some spurious bonding pair density due to its proximity to the axial bonds. The following observations are noteworthy: (1) In all species with Cl/Br/I substituents, the axial halides bend *toward* the lone pair. This also holds for $IO_2F_2^-$. (2) The angle change, the migration of the lone pair closer to I, and the concomitant nonbonded basin volume reduction are clear for $IO_2X_2^-$ even though these are anions and thus presumably contain more diffuse electron density distributions. (3) For $IO_2X_2^-$ anions, the V/e^- values are similar to those of SX_4 compounds, even though the former are anions.

identified with regions in space where electrons are localized. This differs from the traditional valence bond picture in which electron domains are identified with electron pairs, thus avoiding a common student misconception that multiple bonds must add multiple electron domains that repel each other within the VSEPR model. The ELF can be analyzed topologically to divide space into distinct "basins" in which electrons are localized. Basins are classified as "bonded" if they contain more than one atomic nucleus or "nonbonded" (corresponding to a lone pair) if they do not.[38,39] Topological basins are not constrained to a two-electron occupancy, but a relative measure of "lone pair size" may be defined by dividing the defined volume of a nonbonded topological basin on the central atom by the integrated electron density found within that basin, a value referred to as V/e^- hereafter.[40] In this way, it is possible to test the VSEPR repulsion hierarchy by comparing trends in nonbonded basin sizes across substituent

https://doi.org/10.1021/acs.jchemed.3c00415
J. Chem. Educ. 2023, 100, 3659−3666

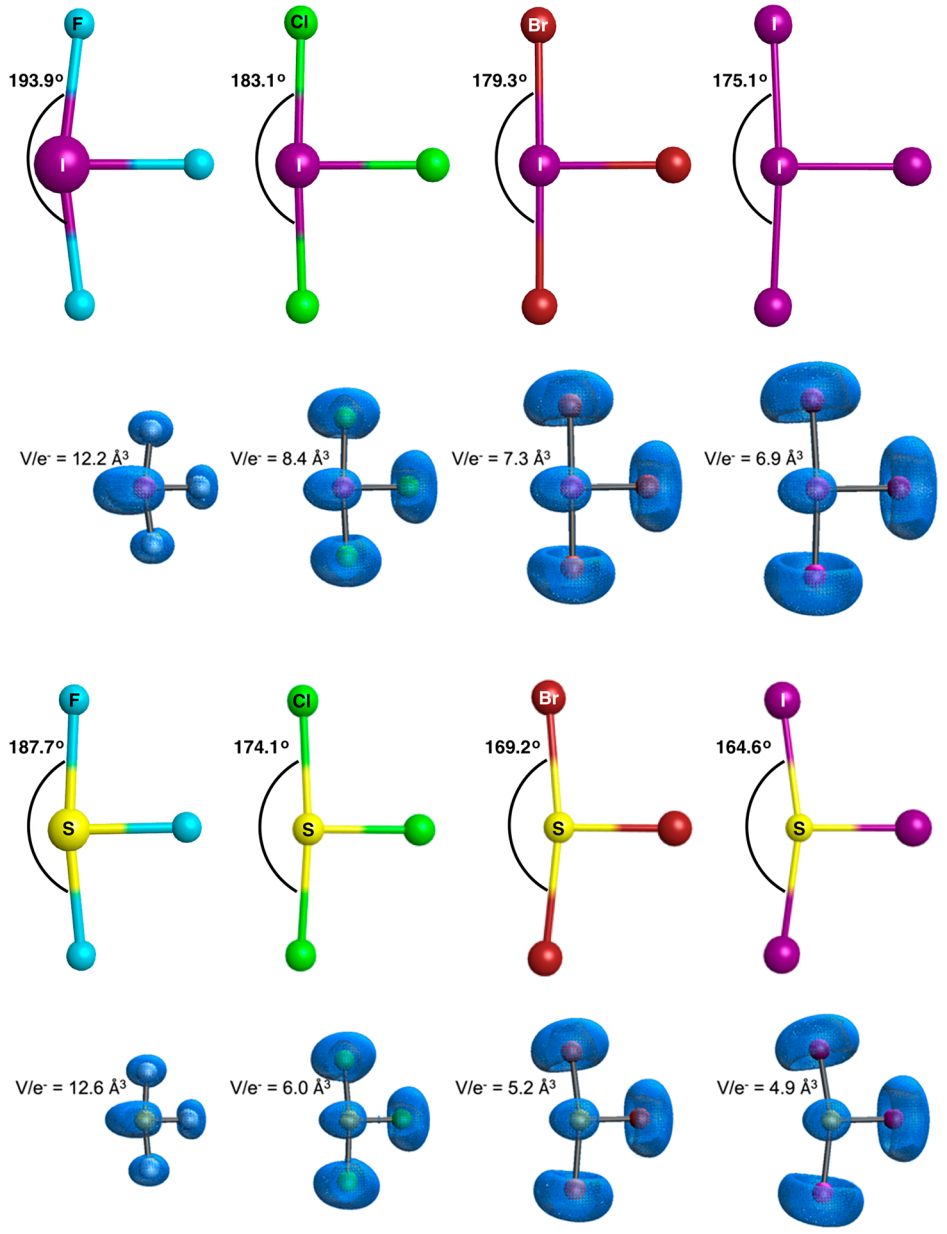

Figure 3. Optimized (M06-2X+GD3/def2-TZVP) structures and associated ELF isosurfaces (η = 0.8) of (top) IX_3 and (bottom) SX_3^- (X = F, Cl, Br, I) showing the change in the X_{axial}–A–X_{axial} angle with halide substituent size. Sulfurs are yellow, fluorines are aqua, chlorines are green, bromines are red-brown, and iodines are purple. The lone pair on A points to the left, and the corresponding nonbonded basins extend to the left of A. V/e^- = the nonbonded basin volume per electron (η = 0.02). It is noteworthy that (1) the angle change and the nonbonded basin migration closer to A and concomitant volume reduction are more pronounced for SX_3^- than for IX_3, even though the former are anions and so presumably contain more diffuse electron density distributions; (2) V/e^- values for IX_3 are generally larger than those for corresponding SX_3^- despite the latter being anions.

and central atom sizes and to examine how these correlate with deviations of bond angles from VSEPR predictions.

We computationally optimized a wide range of hypercoordinate main-group $AX_nE_z^c/AO_mX_nE_z^c$ compounds and ions (A = main-group central atom, X = halide, E = lone pair on central atom, c = charge). We found that while fluorinated species tend to follow the normal VSEPR behavior (with some interesting exceptions), halide homologues more commonly adopt "reverse VSEPR" geometries. It appears this "reverse VSEPR repulsion hierarchy" is characteristic rather than exceptional. Further, a periodic trend in bond angles emerges upon substitution with heavier halides. This trend is consistent with both the increased size and decreased electronegativity of the heavier halides. We provide a high-level quantum-mechanical analysis, including ELF topological basins as a basis for interpretation and evaluation of lone pair volumes. Finally, we suggest a general-chemistry-level conceptualization and propose textbook language to update and improve the presentation of this aspect of VSEPR to students.

RESULTS AND DISCUSSION

Computational methods employed and tabulated angle data are available in the Supporting Information. Of 125 $AX_nE_z^c/AO_mX_nE_z^c$ anions/neutrals examined (A = main-group central atom, X = halide, E = lone pair on central atom, c = charge),

https://doi.org/10.1021/acs.jchemed.3c00415
J. Chem. Educ. 2023, 100, 3659−3666

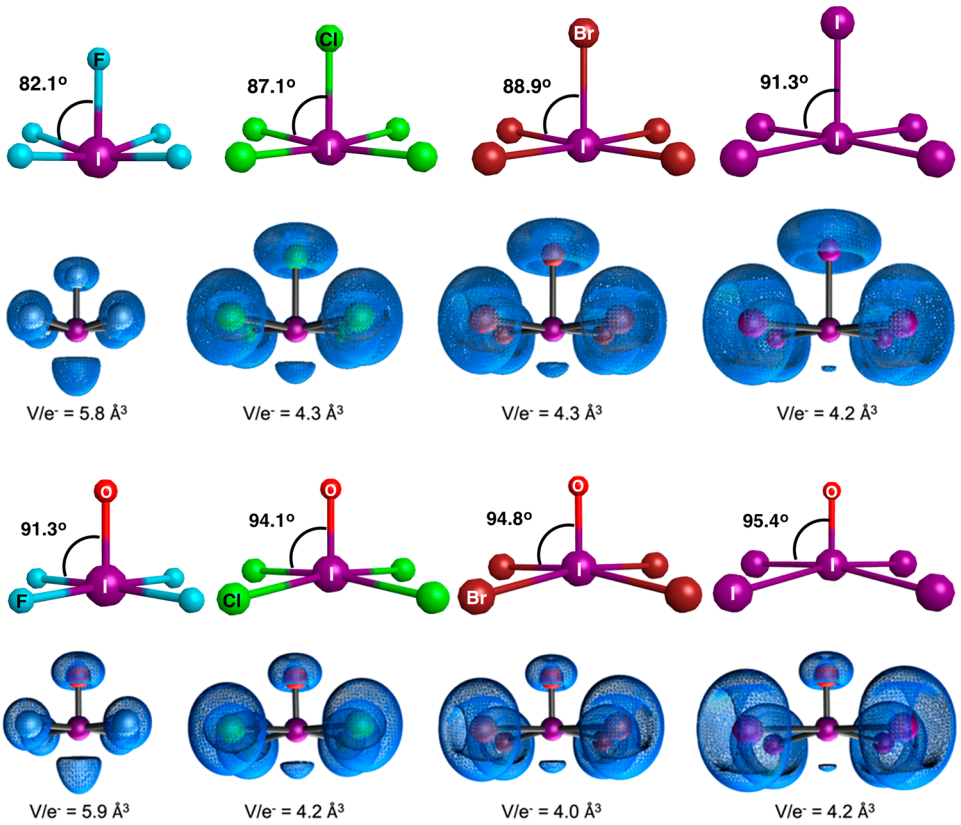

Figure 4. Optimized (M06-2X+GD3/def2-TZVP) structures and associated ELF isosurfaces (η = 0.8) of (top) IX_5 and (bottom) IOX_4^- (X = F, Cl, Br, I) showing the change in the $X_{axial}–I–X_{equatorial}/O–I–X_{equatorial}$ angle with halide substituent size. Oxygens are shown in red, fluorines in aqua, chlorines in green, bromines in red-brown, and iodines in purple. The lone pair on A points to the left, and the corresponding nonbonded basins extend to the left of A. V/e^- is the lone pair basin volume per electron (η = 0.02). For IOI_4^-,V/e^- appears to include some spurious bonding pair density due to its proximity to the axial bonds. The following observations are noteworthy: (1) In all four IOX_4^- cases, the halides point *toward* the lone pair. (2) Nonbonded basin migration closer to I and concomitant volume reduction are similar for IX_5 and IOX_4^- even though the latter are anions and thus presumably contain more diffuse electron density distributions.

88 (70%) exhibited structures inconsistent with the VSEPR repulsion hierarchy. A graphic comparing bond angle data for "normal coordinate" SX_2 with those for hypercoordinate SX_3^- and SX_4 appears in Figure 1; graphics showing additional hypercoordinate examples appear in Figures 2–4. The essential observation to be taken from the calculations is that the models always predict that as the halides get heavier in hypercoordinate $AX_nE_z^c/AO_mX_nE_z^c$ species, at some point those with heavier halides adopt "reverse VSEPR" structures where the peripheral atoms orient toward the lone pair(s) rather than away from it/them. In some cases (Figures 2 and 4), even the fluorides do this. This contradicts VSEPR theory as it is currently presented to students, calling for an update to the theory and its presentation.

We sought a quantum-mechanical explanation for these observations. For each molecule, the ELF was calculated, and an isosurface was generated at the ELF value of 0.8 to visualize electron localization. Graphics showing these isosurfaces appear with the associated structures in Figures 2–4. A more accurate isosurface was then generated at the ELF value of 0.02 and topologically analyzed to obtain volumes and integrated electron populations of nonbonded basins. Topological analysis does not always yield integrated populations of two electrons in each basin, so normalized nonbonded basin volumes per electron (V/e^- values) are reported. One essential observation to be taken from the isosurfaces and normalized V/e^- values is that these basins (and corresponding lone pairs) migrate closer to the central atom and are localized into smaller volumes as the halides get heavier in each set, consistent with Bent's rule. The other (Figure S1) is that nonbonded basins migrate closer to the central atom and are localized into smaller volumes in hypercoordinate sulfur halides than in normal coordinate sulfur halides. Among hypercoordinate species (Figures 2–4), those with "reverse VSEPR" geometries typically yielded calculated V/e^- values smaller than those of similar structures that did not exhibit "reverse VSEPR" geometries. Figure 2 shows that SF_4 has a normalized V/e^- of 8.8 A^3, but all other SX_4 compounds have "reverse VSEPR" geometries and V/e^- = 3.6–3.9 A^3. Similarly, Figure 3 shows that SF_3^- has a normalized V/e^- of 12.6 A^3, but all other SX_3^- anions have "reverse VSEPR" geometries and V/e^- = 4.9–6.0 A^3. Hypercoordinate iodine species in Figures 2–4 also follow this trend, but with a less dramatic volume reduction that may reflect the larger central atom radius.

Chemical intuition and much experimental data hold that the electron density distributions of anions are more diffuse than those of similar electrically neutral compounds.[41] While this should increase basin volumes generally, these calculations suggest that the net effect of a negative charge increases basin volumes toward peripheral atoms more dramatically than those of nonbonded basins on the central atoms for these hypercoordinate species. Somewhat surprisingly, some anionic species with "reverse VSEPR" geometries were found to have

https://doi.org/10.1021/acs.jchemed.3c00415
J. Chem. Educ. 2023, 100, 3659–3666

normalized V/e^- values similar to *or smaller than* those of similar electrically neutral compounds with normal geometries. Figure 4 shows that IOX_4^- anions have comparable V/e^- values to the corresponding IX_5 compounds, while Figure 3 shows that SX_3^- anions have generally smaller V/e^- values than the corresponding IX_3 compounds. This is consistent with a Pimentel–Rundle three center–four electron bonding model that localizes negative charge on peripheral atoms, especially those bonded linearly or near-linearly.[42] Partial charges calculated using natural population analysis also predict that negative charge is localized on these atoms (Table S5).

Hypercoordinate species with peripheral oxygen substituents, such as the experimentally characterized $XeOF_4$, exhibit greater tendencies for peripheral halides to orient toward the lone pair. Figure 4 shows that equatorial halides in IOX_4^- anions bend further toward the lone pair than in the corresponding IX_5 compounds, despite nearly identical V/e^- values. A similar trend is seen in Figure 2 for $IO_2X_2^-/SX_4$. Here, as in the example of SO_2, strong bonding to peripheral oxides, whether as a result of multiple bonding[13] or a high degree of bond polarization or both, apparently competes against steric pressure to increase the likelihood of "reverse VSEPR" geometries.

CONCLUSIONS AND SUGGESTED TEXTBOOK TEXT

VSEPR is based on a concept of mutual repulsion between electron domains, and it is useful for predicting idealized three-dimensional molecular shapes that maximize the space available to each electron domain. For normal coordinate molecules, a pattern emerges whereby nonbonded domains take up more space around the central atom because nonbonded electrons only repel other electron pairs; they are not attracted to any peripheral atoms. This is explained in terms of increased repulsion between lone pair domains and other domains and gives rise to the textbook trend: lone pair–lone pair > lone pair–bonding pair ≫ bonding pair–bonding pair. However, in some experimentally observed hypercoordinate species and computationally predicted geometries for related species, while VSEPR correctly predicts the basic shapes, bond angles are found to be inconsistent with those predicted by the repulsion trend. Thus, the VSEPR principle that lone pairs always occupy more space than bonding pairs around the central atom, or equally that electrons in nonbonded domains exert increased repulsion compared to those in bonding domains, breaks down. As an illustration, for SBr_4 to adopt the structure predicted computationally, the electrons in the axial and equatorial S–Br bonding domains (the S–Br bonds) must repel each other more than they are repelled by the electrons in the equatorial nonbonded domain (the S lone pair). This clearly contradicts the textbook trend.

A more nuanced view can be provided by altering the radial degree of freedom and by focusing on attraction between electrons in lone pairs and the nucleus of the central atom. Hypercoordinate species typically have longer bonds than normal coordinate species, freeing up space closer to the nucleus of the central atom for its lone pairs. Nonbonded electrons closer to the central atom occupy domains with a smaller volume, which in turn reduces their repulsion from electrons in bonding electron domains. Thus, in hypercoordinate species, electrons in lone pair domains might not repel more than those in bonding domains. Although VSEPR correctly predicts the basic shape of hypercoordinate species, its prediction of increased repulsion by lone pair domains breaks down.

As noted above, hypercoordinate species are not the only known examples of geometries in which the peripheral atoms bend toward the lone pair rather than away. H_3O^+ and NH_3 follow the octet rule and are trigonal-pyramidal, but the former has H–O–H bond angles of 113.6° (greater than the idealized VSEPR tetrahedral bond angle of 109.5°)[43] while in the latter the H–N–H angles are 106.6°.[14] Similarly, bent H_2F^+ and H_2O exhibit H–F–H angles of 112.2[44] and H–O–H angles of 104.5°, respectively.[14] We plan to address species of this type in an upcoming paper.

We feel that these observations necessitate rewriting of the textbook text associated with VSEPR theory and hypercoordinate species. Students should be taught that VSEPR is a useful model/predictor for many cases but that the structures of polyatomic ions/molecules represent the "lowest energy" choices arising from multiple factors, of which electron pair repulsion is only one. The assumption that electron–electron repulsion dominates the structural choice does not hold for many known and potential species. $AX_nE_z^c/AO_mX_nE_z^c$ species represent a sizable class for which the exceptions appear to be more common than the "rule". Below is an excerpt from section 7.1, "Deviations from Ideal Bond Angles", in *Chemistry: Atoms First* by Burdge and Overby.[3] We include modified language (in bold) to reflect the information above.

> ***Deviation from Ideal Bond Angles***
>
> *Some electron domains are better than others at repelling neighboring domains. As a result, the bond angles may be slightly different from those shown. For example, the electron-domain geometry of ammonia NH_3 is tetrahedral, so we might predict the H–N–H bond angle to be 109.5°. In fact, the bond angles are about 107°, slightly smaller than predicted. The lone pair on the nitrogen atom repels the N–H bonds more strongly than the bonds repel one another. It therefore "squeezes" them closer together than the ideal tetrahedral angle of 109.5°.*
>
> *In effect, a lone pair takes up more space than the bonding pairs. This can be understood by considering the attractive forces involved in determining the location of the electron pairs. A lone pair on a central atom is attracted only to the nucleus of that atom. A bonding pair of electrons, on the other hand, is simultaneously attracted by the nuclei of both of the bonding atoms. As a result, the lone pair has more freedom to spread out and a greater capacity to repel other electron domains. Also, because they contain more electron density, multiple bonds repel more strongly than single bonds.*
>
> ***In hypercoordinate species, lone pairs do not necessarily repel bonds more strongly than the bonds repel each other. Computational studies suggest that in many cases the opposite is true, and some experimental support for this exists. For example, both experimental and computational studies indicate that the axial fluorines in SF_4 should bend away from the equatorial lone pair. However, computational studies of SBr_4 and SI_4 indicate that the axial halides in each will bend toward the lone pair. The bonding pairs repel each other more strongly than the lone pair repels them. Experimentally, the crystal structure of isoelectronic PBr_4^- supports this, in that the axial bromines point toward the lone pair.***

https://doi.org/10.1021/acs.jchemed.3c00415
J. Chem. Educ. 2023, 100, 3659–3666

While the basis underlying this phenomenon is beyond the scope of this text, one can view it as resulting from the combination of the large size of the heavier halide substituents and the unusually large number of substituents. In hypercoordinate structures, a competition exists between lone pair−bonding pair repulsions and bonding pair−bonding pair repulsions. The former win when the substituents are smaller, and the latter win when the substituents are larger. Thus, one must take the number and size of the substituents into account when predicting whether bond angles may or may not exceed the ideal bond angle, and such predictions should be compared to actual experimental data.

■ ASSOCIATED CONTENT

Supporting Information

The Supporting Information is available at https://pubs.acs.org/doi/10.1021/acs.jchemed.3c00415.

ELF isosurfaces, tables of optimized bond distances and angles, and partial charges from natural population analysis calculations (PDF, DOCX)

■ AUTHOR INFORMATION

Corresponding Authors

Thomas M. Gilbert − *Department of Chemistry & Biochemistry, Northern Illinois University, DeKalb, Illinois 60115, United States;* orcid.org/0000-0003-2053-9655; Email: tgilbert@niu.edu

Christine M. Morales − *Department of Chemistry, Hawaii Pacific University, Kaneohe, Hawaii 96744, United States;* Present Address: Department of Chemistry, Biochemistry, and Physics, University of Mount Union, Alliance, OH, 44601, United States; orcid.org/0000-0001-5813-7219; Email: moralech@mountunion.edu

Author

Annika L. Medrano − *Department of Chemistry, Hawaii Pacific University, Kaneohe, Hawaii 96744, United States*

Complete contact information is available at: https://pubs.acs.org/10.1021/acs.jchemed.3c00415

Notes

The authors declare no competing financial interest.

■ ACKNOWLEDGMENTS

This study did not receive any specific grant from funding agencies in the public, commercial, or not-for-profit sectors. The Northern Illinois University (NIU) Computational Chemistry Laboratory was created using funds from the U.S. Department of Education and is supported in part by the taxpayers of the State of Illinois. The work used resources of the Center for Research Computing and Data (CRCD) at NIU, specifically the Gaea computer cluster. We thank Sergey Uzunyan and Dave Ulrick of CRCD-NIU for their assistance and troubleshooting efforts. Some computational resources were provided by NSF-MRI Award CHE-1039925 through the Midwest Undergraduate Computational Chemistry Consortium (MU3C). Some calculations were performed at the Ohio Supercomputer Center under Project PAA-0003. A.L.M. thanks the Islands of Opportunity Alliance (NSF Grant HRD 1826864) for funding through the Louis Stokes Alliance for Minority Participation.

■ REFERENCES

(1) Gillespie, R. J.; Hargittai, I. *The VSEPR Model of Molecular Geometry*; Allyn & Bacon: Boston, 1991.

(2) Gillespie, R. J.; Hargittai, I. *The VSEPR Model of Molecular Geometry*; Dover Publications: Mineola, NY, 2012.

(3) Burdge, J.; Overby, J. *Chemistry: Atoms First*, 4th ed.; McGraw-Hill: New York, 2021; Chapter 7.1.

(4) Esselman, B. J.; Block, S. B. VSEPR-Plus: Correct Molecular and Electronic Structures Can Lead to Better Student Conceptual Models. *J. Chem. Educ.* **2019**, *96*, 75−81.

(5) Clauss, A. D.; Nelsen, S. F.; Ayoub, M.; Moore, J. W.; Landis, C. R.; Weinhold, F. Rabbit-ears hybrids, VSEPR sterics, and other orbital anachronisms. *Chem. Educ. Res. Pract.* **2014**, *15*, 417−434.

(6) Gillespie, R. J. A defense of the valence shell electron pair repulsion (VSEPR) model. *J. Chem. Educ.* **1974**, *51*, 367−370.

(7) McNaught, I. J. Testing and Extending VSEPR with WebMO and MOPAC or GAMESS. *J. Chem. Educ.* **2011**, *88*, 421−425.

(8) Bock, H.; Goebel, I.; Havlas, Z.; Liedle, S.; Oberhammer, H. Triisopropylamine: A Sterically Overcrowded Molecule with a Flattened NC_3 Pyramid and a "p-Type" Nitrogen Electron Pair. *Angew. Chem., Int. Ed.* **1991**, *30*, 187−190.

(9) Liedle, S.; Mack, H. G.; Oberhammer, H.; Imam, M. R.; Allinger, N. L. Gas-phase structures of di-*tert*-butyl ether and *tert*-butyl methyl ether. *J. Mol. Struct.* **1989**, *198*, 1−15.

(10) Tsuboyama, A.; Konaka, S.; Kimura, M. Molecular structure of di-*tert*-butyl sulfide as determined by gas electron diffraction. *J. Mol. Struct.* **1985**, *127*, 77−83.

(11) Gillespie, R. J.; Popelier, P. L. A. *Chemical Bonding and Molecular Geometry*; Oxford University Press: New York, 2001.

(12) Purser, G. H. The Significance of the Bond Angle in Sulfur Dioxide. *J. Chem. Educ.* **1989**, *66*, 710−713.

(13) Suidan, L.; Badenhoop, J. K.; Glendening, E. D.; Weinhold, F. Common Textbook and Teaching Misrepresentations of Lewis Structures. *J. Chem. Educ.* **1995**, *72*, 583−586.

(14) Miessler, G. L; Fischer, P. J.; Tarr, D. A. *Inorganic Chemistry*, 5th ed.; Pearson: Upper Saddle River, NJ, 2014; Chapter 3.2.

(15) Bent, H. A. Distribution of Atomic *s* Character in Molecules and Its Chemical Implications. *J. Chem. Educ.* **1960**, *37*, 616−624.

(16) Coulson, C. A. *Valence*, 2nd ed.; Oxford University Press, 1961; pp 203−205.

(17) Jensen, W. B. The Origin of the Term "Hypervalent". *J. Chem. Educ.* **2006**, *83* (12), 1751−1752.

(18) Reed, A. E.; Schleyer, P. v R. Chemical Bonding in Hypervalent Molecules. The Dominance of Ionic Bonding and Negative Hyperconjugation over d-Orbital Participation. *J. Am. Chem. Soc.* **1990**, *112*, 1434−1445.

(19) Weinhold, F.; Landis, C. R. *Valency and Bonding: A Natural Bond Orbital Donor-Acceptor Perspective*; Cambridge University Press: Cambridge, U.K., 2005.

(20) Jackson, B. A.; Harshman, J.; Miliordos, E. Addressing the Hypervalent Model: A Straightforward Explanation of Traditionally Hypervalent Molecules. *J. Chem. Educ.* **2020**, *97*, 3638−3646.

(21) Cooper, D. L.; Cunningham, T. P.; Gerratt, J.; Karadakov, P. B.; Raimondi, M. Chemical Bonding to Hypercoordinate Second-Row Atoms: d Orbital Participation versus Democracy. *J. Am. Chem. Soc.* **1994**, *116*, 4414−4426.

(22) Woon, D. E.; Dunning, T. H., Jr. Theory of Hypervalency: Recoupled Pair Bonding in SF_n (n = 1−6). *J. Phys. Chem. A* **2009**, *113*, 7915−7926.

(23) Noury, S.; Silvi, B.; Gillespie, R. J. Chemical Bonding in Hypervalent Molecules: Is the Octet Rule Relevant? *Inorg. Chem.* **2002**, *41*, 2164−2172.

(24) Kimura, K.; Bauer, S. H. Electron diffraction study of the molecular structures of sulfur tetrafluoride (SF_4) and thionyl tetrafluoride (SOF_4). *J. Chem. Phys.* **1963**, *39*, 3172−3178.

(25) Tolles, W. M.; Gwinn, W. D. Structure and Dipole Moment for SF_4. *J. Chem. Phys.* **1962**, *36*, 1119−1121.
(26) Bowater, I.C.; Brown, R.D.; Burden, F.R. The Microwave Spectrum, Dipole Moment, and Structure Analysis of Selenium Tetrafluoride. *J. Mol. Spectrosc.* **1968**, *28*, 454−460.
(27) Shlykov, S. A.; Giricheva, N. I.; Titov, A. V.; Szwak, M.; Lentz, D.; Girichev, G. V. The Structures of Tellurium(IV) Halides in the Gas Phase and as Solvated Molecules. *Dalton Trans.* **2010**, *39*, 3245−3255.
(28) Blake, A. J.; Pulham, C. R.; Greene, T. M.; Downs, A. J.; Haaland, A.; Verne, H. P.; Volden, H. V.; Marsden, C. J.; Smart, B. A. Structure of Tetramethyltellurium(IV) Determined Experimentally in the Solid and Gas Phases and by Ab Initio Calculations. *J. Am. Chem. Soc.* **1994**, *116*, 6043−6044.
(29) Martins, J. F.; Wilson, E. B., Jr. The Microwave Spectrum, Molecular Structure and Dipole Moment of Xenon Oxytetrafluoride. *J. Mol. Spectrosc.* **1968**, *26*, 410−417.
(30) Hoyer, S.; Seppelt, K. The Structure of IF_3. *Angew. Chem., Int. Ed.* **2000**, *39*, 1448−1449.
(31) Burbank, R. D.; Jones, G. R. Crystal Structure of Iodine Pentafluoride at −80°. *Inorg. Chem.* **1974**, *13*, 1071−1074.
(32) Laval, J.-P.; Boukharrata, N. J. Sodium iodine(V) oxyfluoride, $NaIO_2F_2$. *Acta Crystallogr., Sect. C: Cryst. Struct. Commun.* **2008**, *64*, i47−i49.
(33) Clark, M.; Kellen-Yuen, C. J.; Robinson, K. D.; Zhang, H.; Yang, Z. Y.; Madappat, K. V.; Fuller, J. W.; Atwood, J. L.; Thrasher, J. S. "Naked" SF_5^- anion: The crystal and molecular structure of $[Cs^+(18\text{-crown-}6)_2][SF_5^-]$. *Eur. J. Solid State Inorg. Chem.* **1992**, *29*, 809−833.
(34) Sheldrick, W. S.; Schmidpeter, A.; Zwaschka, F.; Dillon, K. B.; Platt, A. W. G.; Waddington, T. C. The Structures of Hypervalent Phosphorus (III) Anions $P(CN)_{4-n}Br_n^-$. Transition from Ψ-Trigonal-bipyramidal to Ψ-Octahedral Co-ordination and Deviation from Valence Shell Electron Pair Repulsion Theory. *J. Chem. Soc., Dalton Trans.* **1981**, 413−418.
(35) Sheldrick, W. S.; Kiefer, J. Crystal Structure of $[Et_4N][PBr_4]$. Structural Correlation for Halogenophosphates(III). *Z. Naturforsch.* **1989**, *44b*, 609−611.
(36) Oberhammer, H.; Shlykov, S. A. Gas phase structures of chalcogen tetrahalides MX_4 with M = S, Se, Te and X = F, Cl, Br, I. *Dalton Trans.* **2010**, *39*, 2838−2841.
(37) Becke, A. D.; Edgecombe, K. E. A simple measure of electron localization in atomic and molecular systems. *J. Chem. Phys.* **1990**, *92*, 5397−5403.
(38) Silvi, B.; Savin, A. Classification of Chemical Bonds Based on Topological Analysis of Electron Localization Functions. *Nature* **1994**, *371* (6499), 683−686.
(39) Silvi, B.; Gillespie, R. J. The ELF Topological Analysis Contribution to Conceptual Chemistry and Phenomenological Models. In *The Quantum Theory of Atoms in Molecules: From Solid State to DNA and Drug Design*; Matta, C. F., Boyd, R. J., Eds.; Wiley-VCH: Weinheim, Germany, 2007; pp 141−162.
(40) Chesnut, D. B. An Electron Localization Function Study of the Lone Pair. *J. Phys. Chem. A* **2000**, *104*, 11644−11650.
(41) This can be explained by their lower ionization potential that enables higher quantum-mechanical tunneling probabilities across longer distances. For example, see: Simons, J. Molecular Anions. *J. Phys. Chem. A* **2008**, *112*, 6401−6511.
(42) Reference 19 , pp 275−306.
(43) Tang, J.; Oka, T. Infrared Spectroscopy of H_3O^+: The $\nu 1$ Fundamental Band. *J. Mol. Spectrosc.* **1999**, *196*, 120−130.
(44) Fujimori, R.; Hirata, Y.; Morino, I.; Kawaguchi, K. FTIR Spectroscopy of Three Fundamental Bands of H_2F^+. *J. Phys. Chem. A* **2013**, *117*, 9882−9888.

https://doi.org/10.1021/acs.jchemed.3c00415
J. Chem. Educ. 2023, 100, 3659−3666